

Technical Note

Enhanced Fat Suppression Technique for Breast Imaging

Mitsue Miyazaki, PhD,^{1,2*} Andrew Wheaton, PhD,¹ and Shinichi Kitane, MS³

Purpose: To evaluate a new fat suppression technique using multiple fat suppression pulses intended for breast dynamic contrast-enhanced (DCE) imaging using segmented three-dimensional fast field echo (FFE).

Materials and Methods: The effect of multiple spectrally-selective fat suppression radiofrequency pulses was modeled using numerical Bloch-equation solutions for the following fat suppression techniques: spectral-selective inversion recovery (SPIR: one pulse), double fat suppression (DFS: two pulses, combining one SPIR pulse and one CHES pulse), and triple fat suppression (TFS: three pulses, combining one SPIR pulse and two CHES pulses). The simulation data were evaluated in terms of fat suppression performance, scan time, and specific absorption rate (SAR) relative to the SPIR technique. The DFS technique was selected as the optimal technique based on the efficacy of fat suppression versus the costs of scan time and SAR. The DFS technique was compared with SPIR in six volunteer studies using segmented T₁-weighted three-dimensional FFE.

Results: The DFS technique produced sufficient fat suppression using only two segments (two fat suppression shots). Breast DCE precontrast images using DFS presented uniform fat suppression compared with SPIR in both axial and sagittal scans in all six volunteers.

Conclusion: DFS is a promising fat suppression technique for breast imaging even in regions with B₁⁺ inhomogeneity.

Key Words: fat suppression technique; B₁ inhomogeneity; breast dynamic contrast-enhanced imaging; double fat suppression

J. Magn. Reson. Imaging 2013;38:981–986.

© 2012 Wiley Periodicals, Inc.

THE BREAST DYNAMIC contrast-enhanced (DCE) application commonly uses a T₁-weighted segmented three-dimensional (3D) fast field echo (FFE) sequence

(FSPGR or Turbo-FLASH) to acquire dynamic images of contrast uptake (1). This technique requires not only high spatial and temporal resolution, but also good fat suppression. Fat suppression is beneficial because the breast DCE examination requires the subtraction of pre- and postcontrast images to cancel out the background signal of the breasts to observe contrast enhancement. Because the fat signal is strong in the T₁-weighted DCE images, poor fat suppression can result in residual fat signal which may lead to misdiagnosis (2). Furthermore, in cases which require observation of presubtraction source images, well fat-suppressed source images are advantageous to observe the contrast of blood and breast parenchyma.

In segmented FFE, to reduce acquisition time, fat suppression modules are typically applied only once per segment. By using an interleaved or centric phase encode (PE) ordering, the fat suppression effect is greatest for the central portion of *k*-space acquired close to the fat suppression shot. Hence, the greater the number of segments, the greater the fat suppression effect in the image. Thus, a trade-off relationship exists between the number of fat suppression pulses (equivalent to the number of segments) and acquisition time. For DCE experiments, the acquisition time is directly related to the dynamic frame rate.

There are many different fat suppression techniques available on commercial systems; (i) inversion recovery based short-tau inversion recovery (STIR) (3), (ii) frequency-selective techniques, such as chemical shift selective fat suppression (CHES) and spectral-selective inversion recovery (SPIR) techniques (4), (iii) Dixon-based in-phase and out-of-phase techniques (5–7), and water-selective excitation (WET) using binomial pulses (8,9). In general, WET is not common in the DCE examination because of long binomial excitation pulses repeated every TR. In addition, frequency-selective techniques are commonly used clinically, although there is ongoing work investigating Dixon-based (10,11) and water-selective (12) approaches in breast imaging.

Frequency-selective techniques work by saturating and/or inverting fat resonances while leaving water signal (mostly) unperturbed. For a single T₁, the ideal flip angle can be chosen to null fat signal at a given TR. However, in practice, the total fat signal is composed of multiple lipid components, each of which has

¹Toshiba Medical Research Institute, Vernon Hills, Illinois, USA.

²Toshiba Medical Systems Corporation, Otawara Tochigi, Japan.

³Toshiba Medical Engineering, Otawara Tochigi, Japan.

*Address reprint requests to: M.M., Toshiba Medical Research Institute USA, 706 N. Deerpath Drive, Vernon Hills, IL 60061. E-mail: mmiyazaki@tmriusa.com

Received May 18, 2012; Accepted October 2, 2012.

DOI 10.1002/jmri.23932

View this article online at wileyonlinelibrary.com.

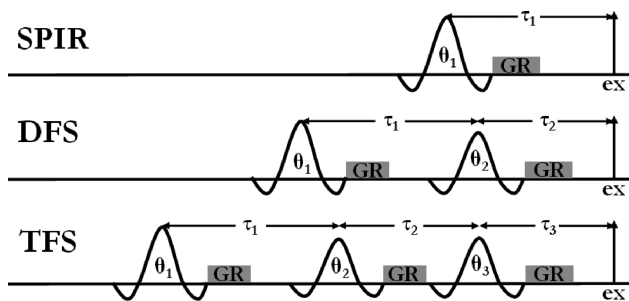


Figure 1. Illustration of pulse sequence diagrams for SPIR (1 pulse), DFS (2 pulses) and TFS (3 pulses) fat suppression modules. Each fat suppression module precedes the initial excitation (ex) of the FFE segment. Each frequency-selective RF pulse is followed by a gradient spoiler (GR) to dephase remaining transverse magnetization. The flip angle (θ) and delay (τ) of each RF pulse can be individually selected.

its own chemical shift, T_1 , T_2 , and relative abundance. Although the fat signal is dominated by the aliphatic methylene (CH_2)_n protons (13), various lipid components like methyl (CH_3) protons with different chemical shift and T_1 may also need to be considered.

Fat suppression in breast imaging is challenging (14), because it suffers from inhomogeneity in static magnetic field (B_0) (15) and transmit radiofrequency (RF) field (B_1^+) (16), both of which are more severe at higher field (3T+). B_1^+ inhomogeneity is caused by the wavelength effect due to the geometry and dielectric characteristics of the breasts resulting in a characteristic asymmetric distribution of the B_1^+ field (2,16). The B_1^+ inhomogeneity deleteriously alters the effective flip angle of the fat suppression RF pulse(s) resulting in imperfect and spatially nonuniform fat suppression in the image (17).

To address the multiple T_1 values of fat, multiple free parameters are required. Thus, additional spectral-selective fat suppression RF pulses, each with an independent flip angle and time delay, are necessary to null the total fat signal. Thus, the use of multiple RF pulses can improve B_1^+ robustness for spectrally-selective suppression (18). Additionally, the spectral-selection bandwidth and/or frequency offset of each RF pulse could be independently adjusted thus affecting the combined spectral suppression profile of the fat suppression module. However, typically the bandwidth and frequency offset are identical for all RF pulses.

In this study, we included additional spectral-selective fat suppression RF pulses to the fat suppression module to create double fat suppression (DFS: two RF pulses, one SPIR pulse and one CHESS pulse) and triple fat suppression (TFS: three RF pulses, one SPIR pulse and two CHESS pulses) (Fig. 1). With the consideration of maintaining the minimum acquisition time for dynamic scanning, we simulated the SPIR, DFS, and TFS techniques using a multi-component model of fat (13). The simulation results were evaluated to choose the optimal technique based on expected level of B_1^+ inhomogeneity, acquisition time, and specific absorption rate (SAR) constraints. Furthermore, the DFS technique was compared with

the conventional SPIR technique in a segmented 3D FFE sequence on healthy volunteers.

MATERIALS AND METHODS

Simulation Modeling

Numerical Bloch-equation solutions for SPIR, DFS, and TFS were used to model the relative fat suppression performance of each technique. The simulation used a multi-component model of human fat where the signal contribution from each fat component was calculated individually using its T_1 and chemical shift at 1.5 Tesla (T) (13). The model included six lipid components, but the dominant signal contribution came from methylene (CH_2)_n (abundance: 0.58 T_1 : 226 ms), methyl CH_3 (abundance: 0.15 T_1 : 577 ms), and allylic $\text{C}=\text{C}-\text{CH}_2$ (abundance: 0.12 T_1 : 209 ms) components.

The numerical solutions were repeated with a range of $\Delta B_1^+ = \pm 20\%$ and number of segments (Nseg) (1, 2, 4, and 8). One application of the fat suppression scheme was applied at the beginning of each segment. The PE ordering was interleaved, meaning that the central PE lines of k -space were closest to the fat suppression application. ΔB_1^+ was incorporated by scaling the flip angle of each RF pulse. All RF pulses were modeled using a spectrally-selective 12 ms 3-lobe sinc RF pulse centered on the methylene resonance (3.4 ppm). Because all RF pulses had the same bandwidth and frequency offset, the spectral selection profile of all three schemes is similar. Thus, ΔB_0 was not included as a dimension to be modeled.

The total fat signal was calculated as the weighted sum of all lipid components. Fat suppression performance was calculated as the ratio of suppressed versus unsuppressed signal. Typical DCE sequence parameters were used in the simulation: TR/TE = 5.5/2.5 ms, FA = 20°, readout (RO) matrix = 256, PE matrix = 240, 140 slices, and PE parallel imaging factor = 2.0. SPIR used a 95° flip angle and 8 ms delay for gradient spoiling. DFS and TFS used an initial 95° RF pulse followed by ($n = 2$ or 3, respectively) 90° pulses each with 4 ms delay times following each pulse (Fig. 1). The total module duration for SPIR, DFS, and TFS was 20 ms, 36 ms and 52 ms, respectively. The effective TI of the SPIR pulse for SPIR, DFS, and TFS techniques was 14 ms, 30 ms, and

Table 1

Acquisition times (seconds) for each fat suppression technique for a range of number of segments*

Technique	No. of slices	No. of segments			
		1	2	4	8
SPIR	80	72.0	73.6	76.8	83.2
DFS	80	73.3	76.2	81.9	93.4
TFS	80	74.6	78.7	87.0	103.7
SPIR	140	95.2	98.0	103.6	114.8
DFS	140	97.4	102.5	112.6	132.7
TFS	140	99.7	107.0	121.5	150.6

*Acquisition times were evaluated using the typical 3D FFE parameters used for simulations and clinical experiments (TR = 5.5 ms, PE matrix = 240, PE parallel imaging factor = 2.0) for number of slices = 80 and 140 (axial and sagittal scans, respectively).

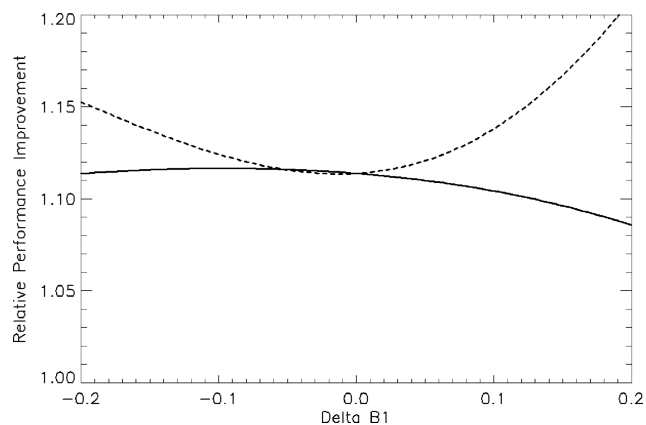


Figure 2. Simulation results on performance of double fat suppression (DFS, solid line) and triple fat suppression (TFS, dashed line) relative to SPIR across a range of $\pm 20\%$ ΔB_1^+ variation. The results indicate on average 10.9% and 13.7% fat suppression performance using DFS or TFS, respectively, as compared to SPIR.

46 ms, respectively. The acquisition time (for each dynamic frame) for each fat suppression technique is listed in Table 1.

Fat Suppression Technique Comparison

For each step of ΔB_1^+ and Nseg, the fat suppression performance of each technique was calculated according to Equation 1 using the SPIR data at Nseg = 1 and $\Delta B_1^+ = 0\%$ as a baseline.

Performance(tech, NSeg)

$$= \frac{\text{FatSignal}(\text{SPIR}, 1) - \text{FatSignal}(\text{tech}, \text{NSeg})}{\text{FatSignal}(\text{SPIR}, 1)}$$

The total scan time for each technique was calculated at each Nseg using the pulse durations and TR described above. SAR was calculated using a pulse energy model. Time-efficiency was calculated as fat suppression performance / scan time and SAR-efficiency was calculated as fat suppression performance / total SAR using the model data. Performance, time-efficiency, and SAR-efficiency data were normalized relative to values of the SPIR data at Nseg = 1 and $\Delta B_1^+ = 0\%$.

MR Imaging

Based on the simulation analysis, the DFS scheme was chosen over the TFS scheme, as later described. Hence, only the DFS scheme was clinically evaluated. The study protocol was approved by the institutional review board and written informed consent was obtained from all six healthy subjects before the experiment. Six healthy female volunteers (mean age, 33.5 years; age range, 24–42 years) were included in the study. The volunteers were confirmed to have no past history or symptom of breast diseases.

MR imaging experiments were performed using a clinical 1.5T system (EXCELART Vantage™/Atlas, Toshiba, Japan), equipped with a 7-ch breast coil. The DFS technique, consisting of the first SPIR pulse

with a flip angle of 95° and a second CHES pulse with 90° , was implemented in 3D FFE with interleaved ordering (the slice encode (SE) direction sequential and the PE direction centric). The frequency offset of all spectrally-selective fat suppression RF pulses were identically centered on the methylene resonance (3.4 ppm).

Six healthy female volunteers underwent both DFS and SPIR experiments. Both axial and sagittal scans were acquired on the same volunteers. Although the sequence design and imaging parameters are designed for DCE, only precontrast data were acquired (i.e., contrast was not administered to the volunteers). For the axial dynamic scans, the following parameters were used: repetition time/echo time (TR/TE) = 5.5/2.5 ms, flip angle (FA) = 15° , matrix = 256 (RO) \times 320 (PE), PE parallel imaging factor = 2.0, field of view (FOV) = 26 \times 36 cm, approximately eighty 2.2-mm section slices (interpolated to 160 1.1-mm slices), resulting in an image resolution of approximately 1.1 \times 1.0 \times 1.1 mm. For the sagittal scans, the following parameters were used; TR/TE = 5.5/2.5 ms, FA = 15° , matrix = 256 (RO) \times 240 (PE), PE parallel imaging factor = 2.0, FOV = 20 \times 20 cm, approximately one hundred forty 2.5-mm section slices (interpolated to 280 1.25-mm slices), resulting in a resolution of approximately 0.9 \times 0.8 \times 1.25 mm. For both axial and sagittal volunteer scans, the scans were repeated using 2 and 4 segments. The scan times for each scenario are listed in Table 1.

RESULTS

The fat suppression performance of DFS and TFS relative to SPIR across the range of ΔB_1^+ is displayed in Figure 2. Over the whole range of ΔB_1^+ , fat suppression performance using DFS and TFS was on average 10.9% and 13.7%, respectively, better than SPIR fat suppression.

The fat suppression performance of each technique as a function of Nseg for the extreme of $\Delta B_1^+ = -20\%$, 0% , and $+20\%$ is plotted in Figure 3a. Performance of TFS was generally better than DFS; both multi-pulse techniques were better than SPIR across all Nseg for all ΔB_1^+ . The inclusion of the extra RF pulses adds scan time as evidenced in Table 1 and Figure 3b. Accordingly, TFS is generally less time-efficient than DFS and SPIR, especially for larger Nseg (> 2), as shown in Figure 3c. At $\Delta B_1^+ = 0\%$, in both performance and time-efficiency, DFS and TFS were generally better than SPIR. Due to the extra RF pulse, TFS is the most SAR-intensive technique and therefore has decreased SAR-efficiency, as shown in Figure 3d. Because TFS offered only slightly better fat saturation improvement than DFS over the range of ΔB_1^+ (13.7% versus 10.9%), but worse time- and SAR-efficiency, DFS was chosen as the technique for further analysis in the phantom and clinical experiments.

Figure 3 shows the effect of fat suppression measured by the signal-to-noise ratio (SNR) in the safflower oil phantom as the number of segments is increased. Increasing the number of segments results in

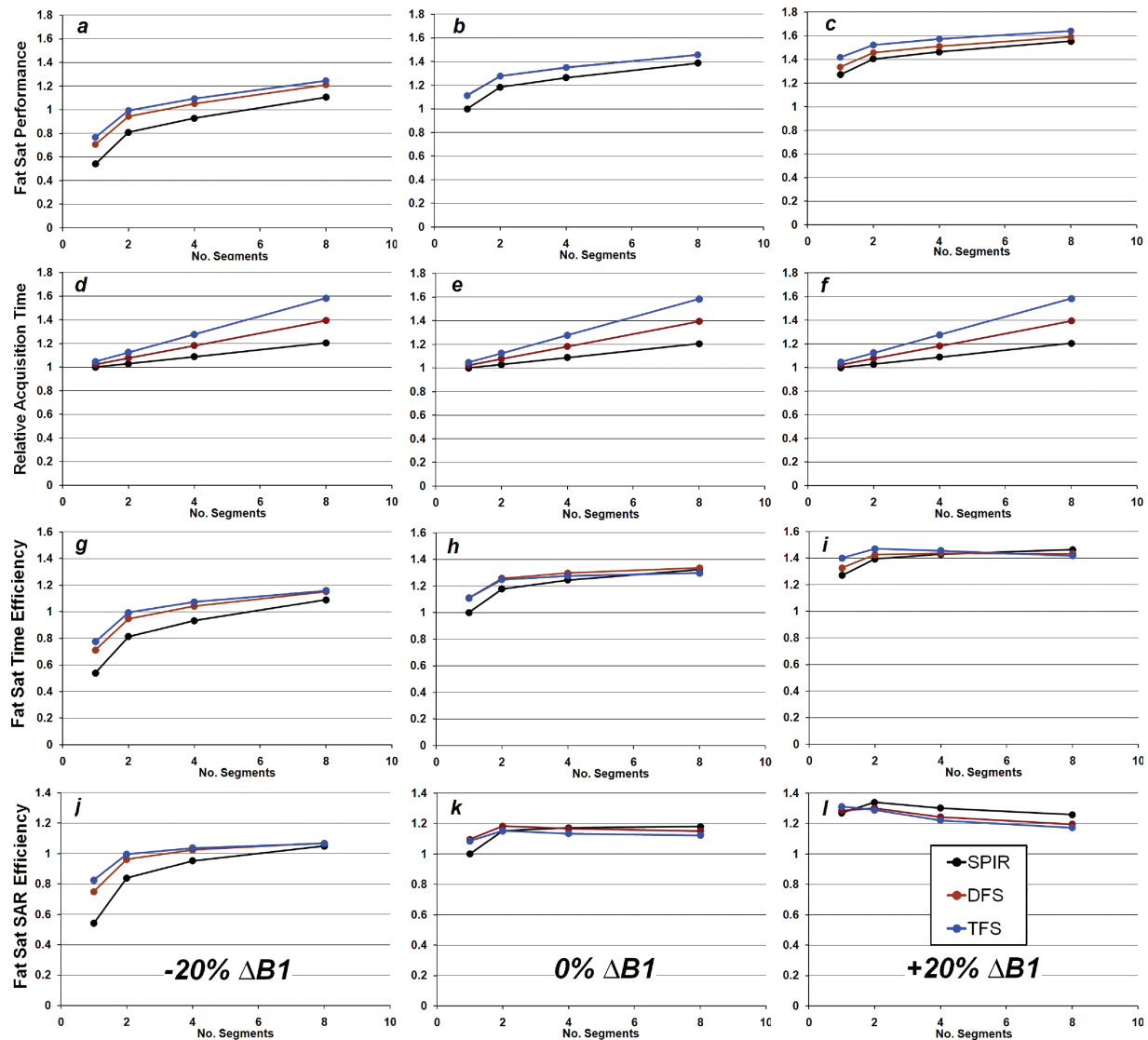


Figure 3. Simulation results of fat suppression performance (a–c), relative acquisition time (d–f), fat suppression time-efficiency (g–i), and SAR-efficiency (j–l) of each technique as a function of the number of segments ($N_{\text{seg}} = 1, 2, 4,$ and 8). Data are plotted separately for $\Delta B_1^+ = -20\%$, 0% , and $+20\%$.

improved fat suppression for both SPIR and DFS. However, fat suppression using DFS is sufficient even with N_{seg} of 2. Figure 4a,b shows the axial breast images obtained using SPIR and DFS, respectively, with N_{seg} of 4. On the axial images, the SPIR technique resulted in adequate fat suppression in most regions, however some regions suffered from uneven fat suppression. In comparison, DFS provided uniform fat suppression throughout the breasts. On the sagittal images, SPIR did not provide the sufficient fat suppression, as shown in Figure 4c. On the other hand, DFS suppressed fat signals uniformly (Fig. 4d). Note that not only the breast fat, but also fat signals around the chest wall are also better suppressed on the DFS image than the SPIR image.

Figure 5 shows the axial and sagittal images of SPIR and DFS using 2 segments. The SPIR technique gives residual fat signal in both axial and sagittal images; while the DFS technique provides uniform fat suppression even using only 2 segments.

DISCUSSION

The idea behind the DFS technique is that the first SPIR pulse suppresses most of the fat signal and the following CHESS pulse suppresses residual fat signal. The T_1 variation of fat signals is seemingly the main cause of the remaining fat signals after application of the first SPIR technique. In addition, for low number of segments ($N_{\text{seg}} < 4$), relatively few central lines of k -space receive full fat suppression; much of k -space is only partially fat suppressed, thus allowing some residual fat signal in the image. The optimal choice of N_{seg} needs to be considered in terms of TR and DCE acquisition time.

Based on the simulation result (Figs. 2 and 3), the fat suppression effect of DFS and TFS is expected to outperform SPIR. In the presence of strong ΔB_1^+ variation, TFS outperforms both DFS and SPIR because the 3rd RF pulse gains B_1 -robustness. In the simulation result of fat suppression performance in the

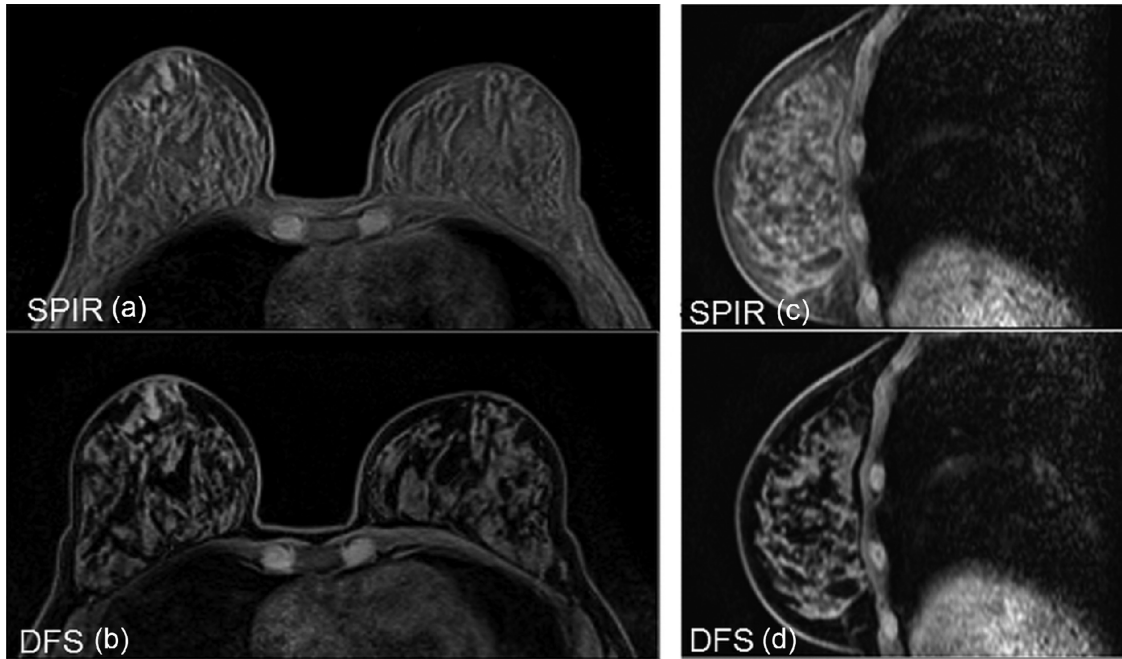


Figure 4. Comparison of breast images of T_1 -weighted 3D FFE using 2 segments in axial orientation (a,b) and sagittal orientation (c,d) using SPIR and DFS. SPIR gives less fat suppression using 2 segments. Even with only 2 segments, DFS provides uniform fat suppressed images in both the axial and sagittal images.

presence of the extreme ΔB_1^+ variation (Fig. 3), the performance of SPIR increases as Nseg increases. However, TFS and DFS gave better performance than SPIR across all Nseg for all ΔB_1^+ variation. Thus, with only a few Nseg, TFS and DFS outperform SPIR. The phantom experiment validated the model conclusion that DFS produces less fat signal compared with SPIR across a range of segments. For small ΔB_1^+ variation, both performance and time-efficiency of TFS and DFS are nearly equal and better than SPIR. With increased ΔB_1^+ variation, TFS works better than DFS and SPIR. However, TFS is less time-efficient than DFS and SPIR (Fig. 3c) with increases in acquisition time of up to 30% for the same number of segments (Fig. 3b). Although TFS is generally less SAR-efficient due to

the extra pulse, for Nseg > 1, the SAR efficiency of all techniques is comparable, with SPIR being the most SAR efficient in many cases.

In the volunteer experiments, DFS produced uniform fat suppression using 2 and 4 segments in the precontrast T_1 -weighted images. Because the RF pulses used in SPIR and DFS shared the same RF waveform and frequency offset, they were all susceptible to the same B_0 off-resonance effects caused by inadequate shim. Thus, the improvement in fat suppression by DFS relative to SPIR is attributed to its B_1^+ robustness and not any frequency selection characteristic of the technique.

The drawback of DFS in the DCE examination is added scan time from the extra time to include the

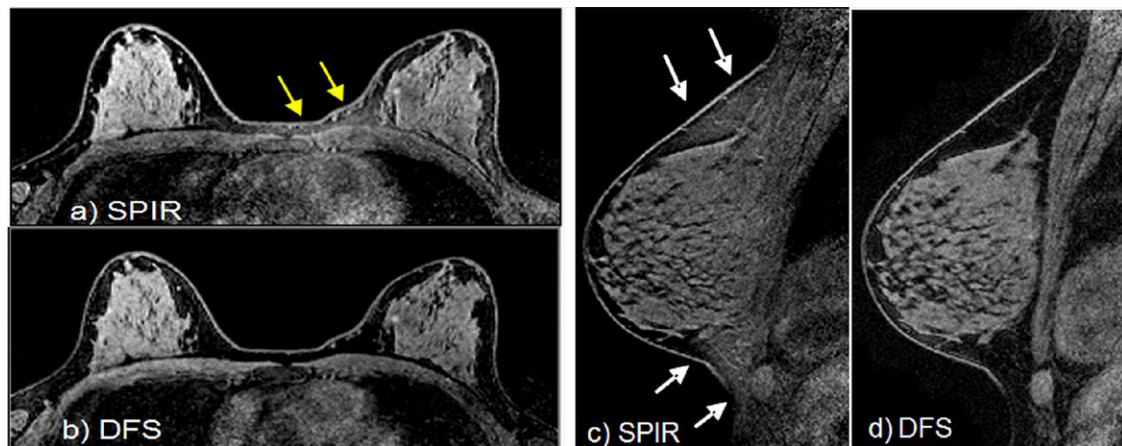


Figure 5. Comparison of breast images of T_1 -weighted 3D FFE using 4 segments in axial orientation (a,b) and sagittal orientation (c,d) using SPIR and DFS. Even with 4 segments, SPIR gives uneven fat suppression in both axial and sagittal images, indicated by arrows in (a) and (c). DFS provides a uniform fat suppression in (b) and (d). [Color figure can be viewed in the online issue, which is available at wileyonlinelibrary.com.]

additional RF pulse and gradient spoiler, which is approximately 16 s. However, the possible reduction in Nseg due to the improved performance of DFS can be leveraged to maintain total scan time without compromising its fat suppression advantages. For example, a two segment DFS is roughly the same acquisition time as a four segment SPIR (Table 1) while providing better fat suppression (Fig. 3a).

We have demonstrated the robustness of DFS in breast DCE imaging at 1.5T. In our breast experiment, DFS produced superb fat suppression in all axial and sagittal acquisitions in all volunteers. At higher field strength (e.g., 3T) and the commensurate increase in B_1^+ inhomogeneity, an additional pulse like TFS may be required to improve the efficiency of fat suppression. In this study, we concentrated on improving fat suppression in breast DCE; however, DFS can be applied in other DCE examinations such as liver, kidney, etc. Furthermore, the application of DFS can be not limited to FFE, but can be applied to other sequences like spin echo (SE), fast spin echo (FSE), single shot FSE, balanced steady state free precession (bSSFP) and so on. In conclusion, the DFS technique provides uniform and superb fat suppression in segmented three-dimensional T_1 -weighted fast field echo images for breast DCE imaging even in regions with high B_1^+ inhomogeneity without compromising scan time.

REFERENCES

1. Turnbull LW. Dynamic contrast-enhanced MRI in the diagnosis and management of breast cancer. *NMR Biomed* 2009;22:28–39.
2. Azlan CA, Di Giovanni P, Ahearn TS, Semple SIK, Gilbert FJ, Redpath TW. B_1 transmission-field inhomogeneity and enhancement ratio errors in dynamic contrast-enhanced MRI (DEC-MRI) of the breast at 3T. *J Magn Reson Imaging* 2010;31:234–239.
3. Bydder GM, Young IR. MR imaging: clinical use of the inversion recovery sequence. *J Comput Assist Tomogr* 1985;9:659–675.
4. Kaldoudi E, Williams SCR, Barker GJ, Tofts PS. A Chemical shift selective inversion recovery sequence for fat-suppressed MRI: theory and experimental validation. *Magn Reson Imaging* 1993; 11:341–355.
5. Dixon WT. Simple proton spectroscopic imaging. *Radiology* 1984; 153:189–194.
6. Glover GH, Schneider E.G.H. Three-point Dixon technique for true water/fat decomposition with B_0 inhomogeneity correction. *Magn Reson Med* 1991;18:371–383.
7. Reeder SB, McKenzie CA, Pineda AR, et al. Water-fat separation with IDEAL gradient-echo imaging. *J Magn Reson Imaging* 2007; 25:644–652.
8. Meyer CH, Hu BS, Nishimura DG, Macovski A. Fast spiral coronary artery imaging. *Magn Reson Med* 1992;28:202–213.
9. Thomasson D, Purdy D, Finn JP. Phase-modulated binomial RF pulses for fast spectrally-selective musculoskeletal Imaging. *Magn Reson Med* 1996;35:563–568.
10. Le-Petross H, Kundra V, Szklaruk J, Wei W, Hortobagyi GN, Ma J. Fast three-dimensional dual echo Dixon technique improves fat suppression in breast MRI. *J Magn Reson Imaging* 2010;31: 889–894.
11. Dogan BE, Ma J, Hwang K, Liu P, Yang WT. T_1 -weighted 3D dynamic contrast-enhanced MRI of the breast using a dual-echo Dixon technique at 3T. *J Magn Reson Imaging* 2011;34:842–851.
12. Niitsu M, Tohno E, Itai Y. Fat suppression strategies in enhanced MR imaging of the breast: comparison of SPIR and water excitation sequences. *J Magn Reson Imaging* 2003;18:310–314.
13. Kuroda K, Oshio K, Mulkern RV, Jolesz FA. Optimization of chemical shift selective suppression of fat. *Magn Reson Med* 1998;40:505–510.
14. Harvey JA, Hendrick RE, Coll JM, Bicholson BT, Burkholder BT, Cohen MA. Breast MR imaging artifacts: how to recognize and fix them. *Radiographics* 2007;27:S131–S145.
15. Bolan PJ, Henry P, Baker EH, Meisamy S, Garwood M. Measurement and correction of respiration-induced B_0 variations in breast 1H MRS at 4 Tesla. *Magn Reson Med* 2004;52:1239–1245.
16. Sacolick LI, Sun L, Vogel MW, Dixon WT, Hancu I. Fast radiofrequency flip angle calibration by Bloch-Siegert shift. *Magn Reson Med* 2011;66:1333–1338.
17. Kuhl CK, Kooijman H, Gieseke J, Schild HH. Effect of B_1 inhomogeneity on breast MR imaging at 3.0 T. *Radiology* 2007;224: 929–930.
18. Ogg RJ, Kingsley PB, Taylor JS. WET, a T_1 - and B_1 -insensitive water suppression method for in vivo localized 1H NMR spectroscopy. *J Magn Reson B* 1994;104:1–10.